JOURNAL OF GEOPHYSICAL RESEARCH, VOL. 106, NO. A8, PAGES 15,767–15,781, AUGUST 1, 2001

Energetic neutral atom imaging of the heliospheric boundary region

Mike Gruntman,[1] Edmond C. Roelof,[2] Donald G. Mitchell,[2] Hans J. Fahr,[3]
Herbert O. Funsten,[4] and David J. McComas[5]

Abstract. Energetic neutral atom (ENA) imaging is a powerful technique, which can remotely probe the properties of distant hot plasmas. Hot plasmas are abundant at the heliospheric boundary, the region where the expanding solar wind meets the surrounding local interstellar cloud. Here we present a new concept for imaging this boundary in ENA fluxes. Heliospheric ENAs are born from charge exchange between energetic protons and the background interstellar atomic hydrogen gas. The technique is ideal for studying the asymmetric three-dimensional heliospheric interface region remotely, from 1 AU. We show that ENA imaging in the 0.2-6 keV energy range will establish the nature of the termination shock and properties of hot proton populations in the heliosheath. We also examine how the evolution of pickup proton populations at and beyond the shock can be explored. Global heliosphere ENA images will distinguish among the competing models of the interaction between the Sun and the local interstellar medium, and they will reveal the physics of important processes in the interface region. Heliospheric ENA fluxes are exceptionally weak, which makes imaging implementation difficult. Nonetheless, we show how single-pixel ENA sensors can image the heliosphere from a spinning spacecraft on a typical mission near 1 AU. The required instrumentation is briefly discussed.

1. Heliosphere

The interaction of the expanding solar wind plasma and local interstellar medium (LISM) creates the heliosphere [*Davis*, 1955; *Parker*, 1963; *Dessler*, 1967; *Axford*, 1972]. The heliosphere is a complex phenomenon where the solar wind and interstellar plasmas, interstellar gas, magnetic fields, and energetic particles all play important roles.

The Sun's interaction with the nearby interstellar medium is of considerable astrophysical interest. Our Sun is typical of its class of stars. Thus the heliosphere offers a unique opportunity to study in detail the only accessible example of a commonplace and fundamental astrophysical phenomenon, the formation of an astrosphere. *Wood and Linsky* [1998] demonstrated the possibility of remotely observing the astrospheres of nearby stars, which opens the possibilities of comparative astrosphere studies.

A possible two-shock Sun-LISM interaction scenario [*Baranov*, 1990; *Baranov and Malama*, 1993, 1995] illustrates the main features of the heliosphere (Figure 1). The interstellar wind approaches the heliosphere with a supersonic velocity and forms the bow shock. The dynamic pressure of the expanding, highly supersonic solar wind decreases with the heliocentric distance. At a certain distance from the Sun this pressure would equal the external LISM pressure of the interstellar wind and magnetic field. The solar wind expansion transitions to a subsonic flow at the termination shock. There the kinetic energy of the supersonic flow is largely converted into thermal energy in the subsonic plasma beyond the shock. This subsonic postshock solar wind plasma flows around the termination shock and down the heliospheric tail. The solar plasma eventually mixes with the interstellar galactic plasma in the tail at distances of 1000-2000 AU.

Interstellar plasma does not penetrate through the heliopause, the discontinuous transition boundary separating the solar and galactic plasmas, but flows around the heliopause. The region between the termination shock and the heliopause is called the heliospheric sheath (heliosheath). Other heliospheric models make somewhat different assumptions, including a subsonic interstellar wind, a weak termination shock, an asymmetric solar wind, and may include an interstellar magnetic field and cosmic rays [e.g., *Fahr and Fichtner*, 1991; *Suess*, 1993; *Linde et al.*, 1998; *Zank*, 1999]. In all the models, the hot shocked solar wind plasma fills the heliosheath and flows down the heliospheric tail.

Three major factors make the heliosphere essentially asymmetric. First, the partially ionized interstellar gas of the LISM moves with a 26 km s^{-1} speed (Figure 1) with respect to the sun (interstellar wind). Second, the interstellar magnetic field could be pointed in any direction. Third, the solar wind is anisotropic with the properties over the Sun's poles significantly different from those close to the ecliptic plane.

The heliosphere has been extensively studied both theoretically and by various experimental techniques since the early 1960s. Experimental data on the region between the supersonic solar wind and the surrounding LISM, the heliospheric interface region, are scarce, mostly indirect, and often ambiguous. Although significant progress was achieved in understanding the Sun-LISM interaction, many important questions are still unanswered, for example: Is the solar wind expansion terminated by a shock? What is the nature of the

[1]Department of Aerospace and Mechanical Engineering, University of Southern California, Los Angeles, California.
[2]Applied Physics Laboratory, Johns Hopkins University, Laurel, Maryland.
[3]Institut für Astrophysik und Extraterrestrische Forschung, Universität Bonn, Bonn, Germany.
[4]Los Alamos National Laboratory, Los Alamos, New Mexico.
[5]Southwest Research Institute, San Antonio, Texas.

Paper number 2000JA000328.
0148-0227/01/2000JA000328$09.00

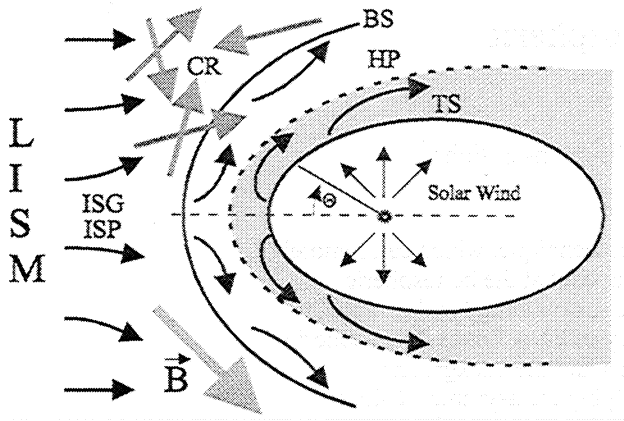

Figure 1. Two-shock model of the interaction of the solar wind with the local interstellar medium. Angle Θ is measured from the upwind direction. The hatched region between the termination shock and the heliopause contains the postshock solar wind plasma and pickup protons. The energetic neutral atoms (ENAs) produced in this region are the focus of this work. LISM, local interstellar medium; TS, termination shock; HP, heliopause; BS, bow shock; CR, cosmic rays; ISP(G), interstellar plasma (gas); B, magnetic field.

termination shock? What is the distance to the shock and its shape? Is the nature of the shock the same in all directions from the upwind (with respect to the interstellar wind) to the downwind? What happens to the solar wind pickup ions at and beyond the shock? We also know very little about the heliopause and the bow shock.

Inferring the properties of the heliospheric interface is complicated by the complexity of the Sun-LISM interaction. The plasma and neutral gas flows are multifluid with often non-Maxwellian ion velocity distributions. Plasmas and neutral atom populations are not in thermodynamic equilibrium, many processes are nonstationary, energetic ions substantially modify the shocks, and galactic and anomalous cosmic rays contribute important pressure gradients. The mean free path of neutral atoms is comparable to the size of the heliosphere, which strongly limits applicability of gasdynamical methods. Consequently, a self-consistent model of the stationary heliosphere has yet to be developed.

The lack of the direct experimental data severely limits our ability to understand the details of the heliospheric interactions. Further progress in studying the Sun-LISM interaction critically depends upon the validation of the fundamental assumptions underlying the concept of the heliosphere. Direct and "clean" experimental data on the nature of the termination shock, its distance and shape, and the evolution of the pickup proton population will substantially advance our understanding of the heliosphere and constrain the competing theoretical models.

Within the next several years, Voyager 1 may reach the termination shock. If so, the spacecraft, now nearing 80 AU, will establish the distance from the Sun to the termination shock in one point direction for a particular phase of the solar cycle. Voyager 1 is headed in approximately the upwind direction, and the termination shock is estimated to be somewhere between 80 and 100 AU [e.g., *Lee*, 1996]. The planned Interstellar Probe spacecraft will cross the termination shock, explore the heliospheric interface, and sample the LISM in approximately the same direction some time after the year 2020. Because the termination shock and the interface region beyond are so huge (hundreds of astronomical units), only remote techniques can provide a global view of the time-varying three-dimensional heliosphere on a continuous basis.

We argue that the technique for obtaining our first information on the global structure of the heliosphere is already at hand. This technique, energetic neutral atom (ENA) imaging, is sensitive to the details of the structure of the heliospheric interface, to the nature of the termination shock, and to the evolution of the pickup proton properties at and beyond the termination shock.

The scientific promise of ENA imaging has been increasingly argued for since the early 1980s and has led to extensive development of the concept and instrumentation. The concept was validated by imaging the magnetospheric ion populations using ad hoc techniques with existing non-ENA instruments [*Roelof*, 1987; *Henderson et al.*, 1997] and dedicated ENA instruments [*Orsini et al.*, 1992; *Mitchell et al.*, 1993, 2000; *Roelof et al.*, 1999; *Brandt et al.*, 1999; *Krimigis et al.*, 2001; *Pollock et al.*, 2000; *Moore et al.*, 2000]. *Williams et al.* [1992] reviewed the concept of magnetospheric imaging, and *Gruntman* [1997] reviewed ENA instrumentation and presented a history of ENA experimental study. Imaging of the heliosphere in ENA fluxes has been advocated for some time [*Gruntman et al.*, 1990; *Gruntman*, 1992, 1997; *Hsieh and Gruntman*, 1993] as a way of exploring remotely properties of the heliospheric sheath plasma. The first dedicated space experiment to detect the heliospheric ENAs was prepared in the mid-1980s [*Gruntman et al.*, 1990] but has never been flown. Complementary EUV mapping of the heliopause is being currently evaluated [*Gruntman and Fahr*, 1998, 2000; *Gruntman*, 2001a, 2001b].

In this article we present the concept of heliosphere imaging using naturally occurring ENA fluxes. ENA imaging will distinguish among the competing Sun-LISM interaction models, radically constrain the models, and explore the physics of the critical and often superimposed processes in the interface region. Heliospheric ENA fluxes are exceptionally weak, which makes imaging implementation nontrivial. Therefore we also describe how the heliosphere can be imaged on a realistic space mission based on the available instrumentation technology.

2. Heliospheric Interface

The properties of the LISM determine important features of the Sun-LISM interaction. The physics of the LISM is far from completely understood [*Cox and Reynolds*, 1987; *Frisch*, 1995; *Breitschwerdt*, 1996]. The LISM is not in thermodynamic equilibrium and may not be in a stationary state, because of the Sun's proximity to the edge of the Local Interstellar Cloud [*Linsky et al.*, 2000]. The LISM velocity vector with respect to the Sun (26 km s^{-1}; ecliptic longitude 252° and latitude +7°) and the LISM temperature (~7000 K) have been reliably established [*Lallement et al.*, 1990; *Witte et al.*, 1996]. However, the inferred number density and the degree to which the LISM is ionized are poorly known; we also know very little about the direction and magnitude of the interstellar magnetic field.

Interstellar plasma and neutral gas are efficiently coupled in the heliospheric interface through charge exchange, which modifies the properties of the inflowing interstellar atoms [*Wallis*, 1975; *Ripken and Fahr*, 1983; *Baranov and Malama*, 1993, 1995; *Lallement et al.*, 1993; *Fahr et al.*, 1995; *Fahr*, 1996; *Izmodenov et al.*, 1997]. The most prominent

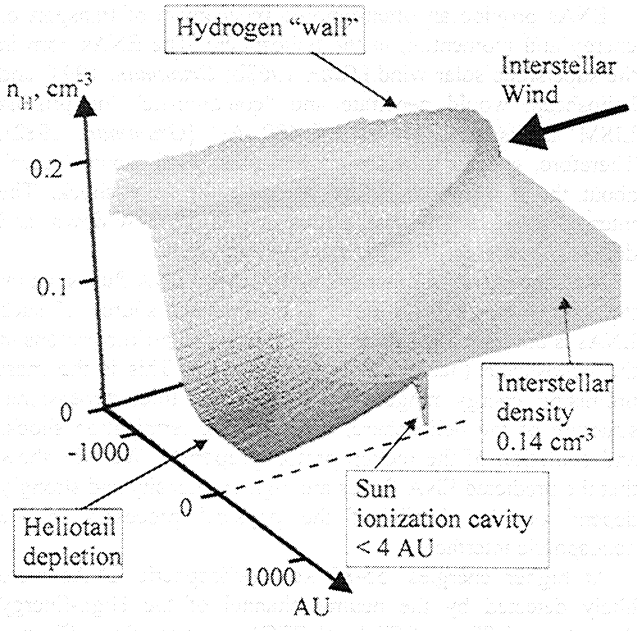

Figure 2. Distribution of interstellar atomic hydrogen. The density enhancement ("hydrogen wall") is the effect of the neutral-plasma charge-exchange coupling. The number density precipitously drops because of the ionization in the Sun's vicinity (solar cavity). Calculations of Baranov and Malama [1993, 1995].

manifestation of this plasma-gas coupling, depicted in Figure 2, is an upwind enhancement (hydrogen wall) and downwind depletion of the atomic hydrogen density. The measurements of the hydrogen glow in the 121.6-nm resonance line confirmed the predicted density enhancement and slowing of the interstellar wind [*Lallement et al.*, 1993]. The complexity of the time-varying asymmetric Sun-LISM interaction essentially limits the utility of these glow measurements for revealing the details of the interaction.

The plasma-gas coupling also determines the extension of the heliospheric tail. The initially hot ($\geq 10^6$ K) shocked solar wind plasma enters an extended plasma tail. *Parker's* [1963] original description of this plasma flow was recently generalized by inclusion of charge-exchange reactions with interstellar hydrogen atoms entering the tail from the outer flanks [e.g., *Osterbart and Fahr*, 1992; *Baranov and Malama*, 1993; *Czechowski et al.*, 1995; *Jaeger and Fahr*, 1998]. No experimental data are yet available to test our concepts of the heliospheric tail.

Ionization of heliospheric neutral atoms produces pickup ions in the solar wind [e.g., *Holzer and Axford*, 1970; *Fahr*, 1973; *Vasyliunas and Siscoe*, 1976; *Moebius et al.*, 1985; *Gloeckler et al.*, 1993]. The solar wind plasma approaching the termination shock is in an essentially nonequilibrium state. The plasma consists of three major distinct components, original solar wind protons, solar wind electrons, and pickup protons. All three components have the same bulk velocity but different effective temperatures. In addition, the pickup protons that constitute 10-20% of the solar wind at the shock are essentially non-Maxwellian.

Evolution of the pickup ion velocity distribution function, as the solar wind expands to the termination shock, and the nature of the termination shock are complex and not completely understood phenomena [e.g., *Isenberg*, 1986, 1997a, 1997b; *Fahr and Ziemkiewicz*, 1988; *Bogdan et al.*, 1991; *Yoon et al.*, 1991; *Chalov et al.*, 1995; *Chalov and Fahr*, 1996; *Fahr et al.*, 2000]. Pickup ions provide seed particles [*Fisk et al.*, 1974] for ion acceleration [*Pesses et al.*, 1981] to cosmic ray energies at the termination shock, forming the so-called anomalous cosmic rays. The shock itself is likely modified by pickup ion acceleration in the precursor and subshock regions [*Jokipii and Giacalone*, 1996; *Fisk*, 1996; *Zank et al.*, 1996]. The pickup protons would not only substantially weaken the shock but also modify the energy spectra of anomalous cosmic rays in the shock's vicinity [*Chalov et al.*, 1995, 1997; *Chalov and Fahr*, 1996; *LeRoux and Fichtner*, 1997]. The lack of direct experimental data limits our ability to validate the concepts of particle acceleration at, and the nature of, the termination shock.

3. Termination Shock

We do not know what exactly happens in the region of the heliospheric interface. However, we do know that the solar wind is supersonic at least to the present-day distances of Voyager spacecraft nearing ~80 AU, and we do know that the solar wind supersonic expansion cannot continue indefinitely because of the finite LISM pressure. If the concept of the solar wind termination by a shock is correct, then there is a region containing hot (shocked) decelerated (subsonic) plasma beyond the termination shock. The properties of the postshock plasma would strongly depend on the nature of the shock, i.e., whether the shock is predominantly gasdynamical and strong [e.g., *Baranov*, 1990] or moderated by energetic particles and weak [*Zank et al.*, 1993; *Chalov and Fahr*, 1994, 1996; *Lee*, 1996; *LeRoux and Fichtner*, 1997; *Isenberg*, 1997b; *Fahr and Rucinski*, 1999; *Fahr and Lay*, 2000]. We also do not know how the solar wind energy is redistributed between the proton and electron components of the postshock plasma.

Pickup protons constitute a significant fraction, up to 20%, of the solar wind at the termination shock. The pressure of the pickup ions could significantly weaken or moderate the termination shock. The pickup ions moderate the shock, while the type I and II Fermi processes are believed to accelerate pickup ions, producing even more energetic ions, which would weaken the shock further. Though theoretical modeling provides some insight into proton injection and acceleration at the termination shock, all the experimental data are indirect.

The nature of the shock may also depend on the ecliptic latitude. The typical solar wind speed over the Sun's poles is significantly higher than the speed close to the ecliptic plane, 750 versus 450 km s^{-1} [*Neugebauer*, 1999; *McComas et al.*, 2000a]. Hence an average solar wind proton carries almost 3 times more energy in the polar directions than near the ecliptic. In addition, the ecliptic latitude where the transition from the high-speed to slow-speed flow occurs significantly depends on the solar cycle phase [*Bertaux et al.*, 1996, 1999; *McComas et al.*, 2000a, 2000b].

Solar wind momentum flux is ~50% higher over the sun's poles than near the ecliptic plane. Therefore the termination shock would likely be a factor of ~1.2 farther away over the Sun's poles compared to the ecliptic at the same angle from the upwind direction. The solar wind pickup proton fraction at the shock is roughly proportional to the distance to the termination shock times the charge-exchange cross section. Because the cross section at 750 km/sec is a factor of ~1.2 less than that at 450 km/sec, the pickup proton fraction would be approximately the same. However, the pickup energies would be significantly,

a factor of ~3, different. In addition, the solar wind magnetic field structure dramatically varies with ecliptic latitude. All these variations may translate into fundamental differences of the termination shock at different latitudes and longitudes.

Gasdynamical models of the interaction fail to properly describe non-Maxwellian plasma ion velocity distributions, in particular that of the pickup ions. However, such models are useful for describing the macroscopic properties of plasma flows because they are fundamentally based on conservation laws. Gasdynamical descriptions allow a convenient inclusion of the magnetic field effects [e.g., *Linde et al.*, 1998; *Ratkiewicz et al.*, 1998] and solar wind anisotropy [e.g., *Linde et al.*, 1998; *Zank*, 1999] and self-consistent inclusion of the plasma-neutral gas coupling with the kinetic description of neutral components [*Baranov and Malama*, 1993, 1995]. In the absence of complete self-consistent interaction models, one can describe the pickup proton populations as being convected by the flow field obtained gasdynamically.

4. Heliospheric Energetic Neutral Atoms

ENAs are born in the charge exchange between energetic plasma ions and background neutral gas. When charge exchange occurs, the resulting ENA instantaneously becomes independent from the surrounding plasma and the influences of the magnetic field. The neutral particle moves in a ballistic trajectory away from the point of charge exchange governed only by the initial velocity and gravitational forces. With the exception of very low energies (< 50 eV/nucleon), gravitation can be disregarded, and one can assume that ENAs preserve those energetic ion velocities immediately before the charge-exchange collisions. As ENAs travel through space, they may be lost by ionization in a second charge exchange, electron collisions, and photoionization. ENA loss is usually small and mostly occurs close (<10 AU) to the Sun; elastic collisions (scattering) of ENAs on the solar wind plasma are negligible beyond 1 AU. The ENA ability to fly straight across magnetic field lines and their small and reliably quantifiable loss allow probing of remote, inaccessible regions in space. Additionally, ENA imaging provides the only way to image plasma protons.

It was understood in the early 1960s that the processes at the solar wind termination region would produce ENAs (see review by *Gruntman* [1997]). The emerging concept of the heliosphere [*Davis*, 1955; *Parker*, 1963] was extended in 1963 by *Axford et al.* [1963], who predicted the formation of ENAs in the heliospheric interface, and by *Patterson et al.* [1963], who suggested that about half of the solar wind protons would reenter the solar cavity (with three fourth of the initial solar wind velocity) in the form of hydrogen ENAs. This latter idea was put forward to explain the then-recently discovered [*Morton and Purcell*, 1962; *Patterson et al.*, 1963] atomic hydrogen in interplanetary space.

Fahr [1968a] explained how interstellar neutral atoms could penetrate the heliosphere following the Keplerian trajectories and reach the Sun's vicinity. Measurements of interplanetary glow in the hydrogen and helium resonance lines firmly established that interplanetary space is filled by interstellar gas directly entering the solar system [*Fahr*, 1974; *Holzer*, 1977; *Meier*, 1977; *Thomas*, 1978; *Bertaux*, 1984]. *Gruntman* [1992] showed later that the ENA flux from the heliospheric sheath is highly anisotropic and significantly weaker than was suggested by *Patterson et al.* [1963].

ENAs provide an often-ignored mechanism of transport of energy and momentum in the heliosphere. The ENAs born in the supersonic solar wind [*Fahr*, 1968b; *Gruntman*, 1994] and heliosheath would penetrate and "contaminate" the pristine LISM at distances up to 300-400 AU [*Gruntman*, 1982]. Therefore, even a supersonic interstellar wind would "learn" about the heliosphere before reaching the bow shock. The interstellar wind flow would thus be heated, slow down, and deflect [*Gruntman*, 1982] as shown in Figure 1.

We concentrate in this work on hydrogen ENA fluxes within the energy range 0.2-6 keV. The dominant source of such ENAs is the postshock solar wind plasma and pickup protons in the heliosheath (hatched area in Figure 1). This is the most promising energy range for study of the three-dimensional structure of the heliosphere, nature of the termination shock, and evolution of the pickup proton properties. We will show that the predicted ENA fluxes are high in intensity and strongly depend on the details of the physical processes in the heliospheric interface.

At higher energies, 55-80 keV heliospheric ENAs were likely detected by the neutral channel of the High-Energy Suprathermal Time-of-Flight (HSTOF) sensor of the Charge, Element, and Isotope Analysis System (CELIAS) on Solar and Heliospheric Observatory (SOHO) [*Hilchenbach et al.*, 1998]. The fluxes of such higher-energy ENAs are orders of magnitude smaller than those with E<6 keV. However, ENAs with E>20 keV could open a way [*Hsieh et al.*, 1992; *Roelof*, 1992] to explore the important processes of ion acceleration at shocks to cosmic ray energies. Shocks are known to provide efficient mechanisms for ion acceleration in space plasmas [*Czechowski et al.*, 1995; *Gloeckler et al.*, 1994, 1995; *Keppler et al.*, 1995; *Chalov et al.*, 1997; *Hilchenbach et al.*, 1998; *Chalov and Fahr*, 2000]. The high-energy ENAs are beyond the scope of this work.

5. ENA Production and Loss

The postshock solar wind plasma consists mostly of protons (~ 95%) and alpha particles (~5%), while background neutral interstellar gas consists of hydrogen (~90%) and helium (~10%). The heliospheric ENAs are predominantly hydrogen atoms. The cross-section energy dependences for proton charge exchange on hydrogen and helium are shown in Figure 3. Charge exchange on hydrogen would clearly dominate the production of the heliospheric ENAs with energies below 100 keV.

The details of the calculations of the heliospheric ENA fluxes can be found in the work of *Gruntman* [1992, 1997]. Briefly, the directional differential ENA flux $j_{ENA,i}$ (cm^{-2} s^{-1} sr^{-1} erg^{-1}) of a given species i from a given direction $\vec{s}$ is a line of sight integral

$$j_{ENA,i}(\vec{s},E) = \int_{\vec{s}} j_i(\vec{s},E) \sum_k \left[\sigma_{ik}(E)\, n_k(\vec{s})\right] P(\vec{s},E)\, ds, \quad (1)$$

where $j_i(\vec{s},E)$ is the local directional differential flux of parent ions, $n_k(\vec{s})$ is the local number density of neutral species k of the background gas, and $\sigma_{ik}(E)$ is the energy-dependent charge-exchange cross section between ions of species i and neutrals of species k. The survival probability, P,

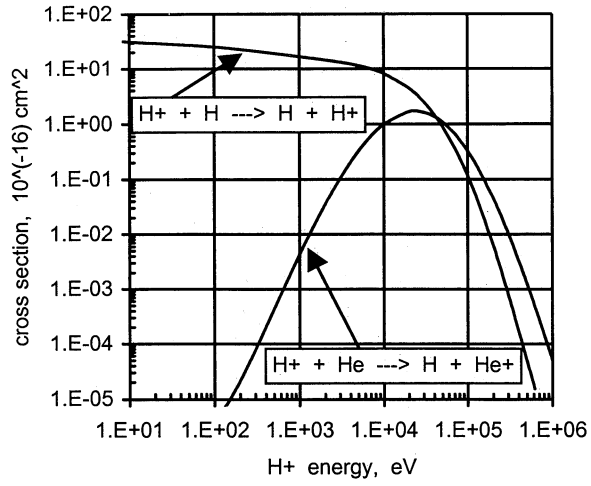

Figure 3. Cross-section energy dependence for proton charge exchange on hydrogen and helium atoms. From *Gruntman* [1997].

of ENAs allowing for particle extinction on their way from their point of birth to the observation point is

$$P(\vec{s},E) = \exp\left[-\int \beta(t)\,dt\right], \qquad (2)$$

where $\beta(t)$ is the ENA total loss rate from charge exchange, electron impacts, and photoionization.

The ionization rate is inversely proportional to the square of the distance from the Sun for R>0.2 AU. The typical rates at 1 AU are $\beta_E = (4\text{-}8)\times10^{-7}$ s^{-1} [e.g., *Fahr*, 1974; *Holzer*, 1977; *Gruntman*, 1994; *Rucinski et al.*, 1996; *McComas et al.*, 1999; *Bertaux et al.*, 1999]. We assume that the ionization rate is constant in time and independent of heliographic latitude and longitude. Figure 4 shows the probabilities of reaching 1 AU for ENAs moving radially toward the Sun and $\beta_E = 6\times10^{-7}$ s^{-1} as a function of the ENA initial (at infinity) energy. The 0.2–6 keV ENAs are of primary interest for the present work. The survival probability is ~ 60% for the ENAs at the low-energy limit, and it gradually increases to 90% at 6 keV.

The differential flux (per unit area and sold angle in unit time) of ENAs with velocity V coming radially toward the Sun to an observer at a point R_0 is given by

$$j_{ENA}(V) = \int_{R_0}^{\infty} N_p(R) N_A(R) f(V,R) \sigma(V) P(V,R_0) V dR, \quad (3)$$

where N_p and N_A are the local proton and neutral number densities, σ is the velocity-dependent charge-exchange cross section, $f(V,R)$ is the local proton velocity distribution function in the observer reference frame, and $P(V,R_0)$ is the probability to reach the observation point without loss.

6. Remote Study of Hot Plasmas

Figure 5 illustrates the concept of remote probing of proton velocity distributions and its sensitivity to plasma temperatures. Let an instrument measuring ENAs in a given velocity (energy) band be pointed in the antisolar direction (Figure 5a). The charge exchange in the supersonic solar wind flow would produce ENAs with the velocities in the antisolar direction (negative V_{ENA}), which could not be measured (Figure 5b). The transition in the termination shock would slow the plasma down and heat the proton population. Many protons would now have the velocities pointed toward the Sun, and some ENAs would be produced within the instrument energy band (Figures 5c-5e). The measured ENA flux would thus strongly depend on the type of the shock.

If the shock is strong (gasdynamical), then the solar wind plasma would significantly slow down and be strongly heated (Figure 5c). If the shock is weak (moderated by energetic ions), then the velocity change and heating would be small (Figure 5e). The expected ENA flux is much higher for the strong shock. A typical instrument would have several energy bands allowing measurement of the distribution of the ENAs with positive velocities.

The energy of protons in the supersonic solar wind is 1-3 keV, while the energy of electrons is a few eV. The gasdynamical models often treat the plasma as a single fluid assuming the same proton and electron temperatures. In the case of a strong shock, a large fraction of the supersonic solar wind kinetic energy is transformed into the thermal energy of the plasma. If most of this energy remains in the plasma proton component, then the proton temperature would be significantly higher than the electron temperature. This uneven energy distribution would be pronounced in ENA energy distributions (Figures 5c and 5d).

The bulk of the pickup protons in the supersonic solar wind upstream of the termination shock does not produce detectable ENAs (Figure 5f). The strength of the termination shock would determine the energy distribution of the ENAs produced by the pickup protons in the downstream region (Figures 5g and 5h). We do not know what exactly happens with the proton velocity distribution in the shock transition, whether it remains unchanged, being compressed, thermalized (Maxwellized), or evolves in some other way. The ENA energy distributions would reveal the pickup proton properties at and beyond the termination shock.

The sensitivity of ENA distributions to proton velocity distributions and bulk velocities makes ENAs a powerful tool to remotely study the properties of hot plasmas. Depending on the direction of the shocked plasma flow in the heliosheath, the flux

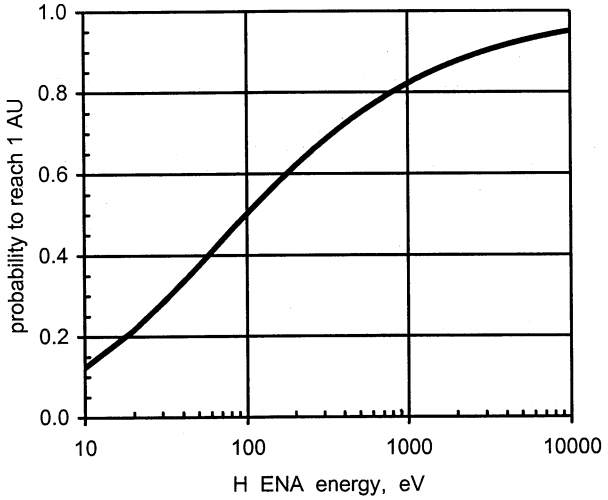

Figure 4. Survival probability for H ENAs to reach 1 AU.

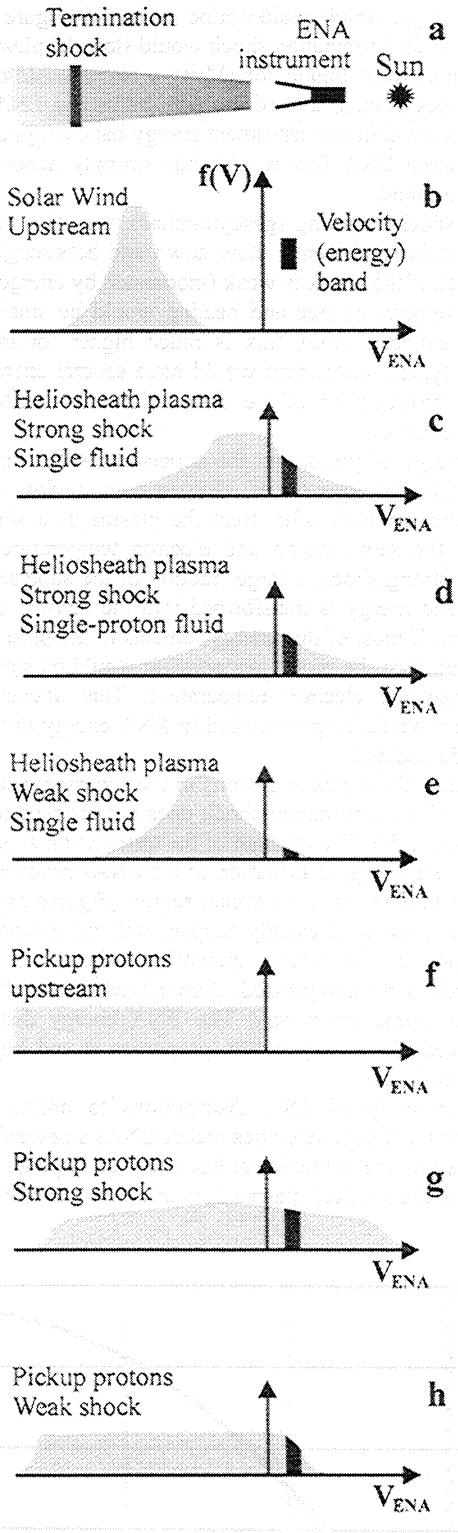

Figure 5. Remote probing of the ion velocity distribution function $f(V)$. (a) Observation geometry. (b) Supersonic (upstream) solar wind. (c) Heliosheath (shocked) plasma and strong shock (single fluid). (d) Heliosheath plasma and strong shock with all the energy confined in the proton component. (e) Heliosheath plasma and weak shock (single fluid). (f) Solar wind pickup protons upstream of the termination shock. (g) Pickup protons in the heliosheath (strong shock). (h) Pickup protons in the heliosheath (weak shock).

of ENAs at a given velocity (energy) would probe different parts of the proton velocity distribution function and may vary by orders of magnitude. ENA spectra are extremely sensitive to the flow pattern in the heliosheath. Global ENA imaging thus gives us spectral information on the nature of the evolution of the proton populations at the termination shock interwoven with the global flow pattern of the plasma in the heliosheath.

The solar wind reaches the termination shock in ~1 year. A hydrogen ENA with energy ~1200 eV would cross back the distance of ~100 AU from the heliospheric sheath and reach an observer in the inner solar system also in 1 year. It would take 2 years for a 300-eV ENA to reach the observer. Therefore the heliospheric images would measure the heliosheath plasma properties averaged over a few years. Therefore heliosphere imaging is capable of probing the 11-year solar cycle variations of the interface region.

7. Model

We demonstrate the main features and potential of heliosphere imaging in the ENA fluxes using a two-shock gasdynamical model [*Baranov and Malama*, 1993, 1995; *Baranov et al.*, 1998]. The two-shock (Baranov) model assumes that both the interstellar plasma flow and the solar wind plasma flow are supersonic. The plasmas are described as single fluids, while the neutral gas is described kinetically. The plasma-gas charge-exchange coupling is treated self-consistently. Cosmic rays, energetic particles, and magnetic field are disregarded. The heliospheric axisymmetric plasma-gas flow fields (velocity, temperature, and number density) were calculated for this work by V. Baranov and his group at the Russian Academy of Sciences, Moscow.

The following LISM parameters (at infinity) are assumed: velocity, 25.0 km s^{-1}; temperature 5672 K; electron (proton) number density n_e = 0.07 cm^{-3}; neutral hydrogen number density n_H = 0.14 cm^{-3}. The solar wind is spherically symmetric with the speed 450 km s^{-1} and number density 7.0 cm^{-3} at 1 AU. The calculated strong termination shock, heliopause, and bow shock are shown in Figure 6. The calculated distribution of neutral hydrogen was shown in Figure 2. By measuring the directional dependence of ENA fluxes, one can construct a composite all-sky image of the heliosphere from inside [*Gruntman*, 1997].

Two major possibilities of the termination of the solar wind expansion are a strong shock and a weak shock. In the case of a strong shock, the two-shock gasdynamical model as described above is applied. The ENA fluxes are calculated using (3) for given plasma local number densities, velocities, and temperatures along the lines of sight. In the case of a weak shock, the bulk of the original solar wind plasma would not be sufficiently heated to produce ENA fluxes with the energies >0.2 keV.

The most prominent source of the higher-energy ENAs with the energies up to a few keV is the pickup protons in the postshock region. Therefore ENA global images would directly reveal the evolution of the pickup proton population at and beyond the termination shock. The details of this evolution could be different over the Sun's poles and near the ecliptic.

We do not know what exactly happens to pickup protons at the shock crossing or later, when they are being evacuated to the heliospheric tail. We consider here two deliberately simple and qualitatively different possibilities. First, we assume that

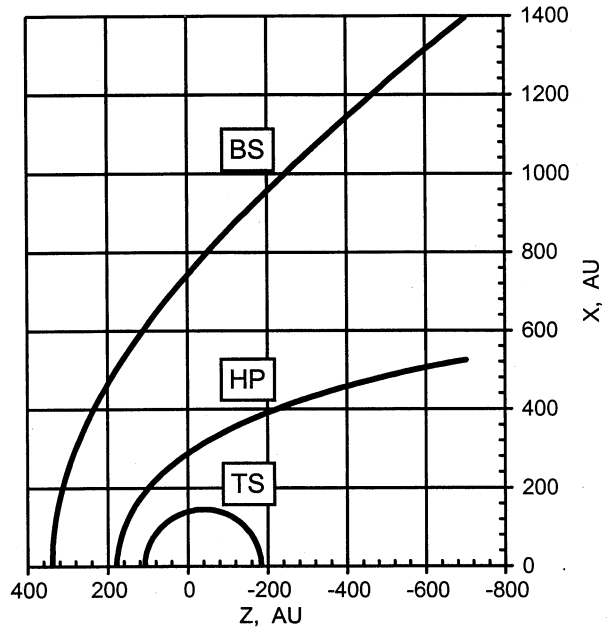

Figure 6. The axisymmetric heliospheric structure used in this work (calculations by *Baranov and Malama* [1993, 1995]). The interstellar wind approaches from the left along the *Z* axis. BS, bow shock; HP, heliopause; TS, termination shock.

the pickup proton velocity distribution function in the solar wind is a uniformly filled sphere in the velocity space with the diameter equal to $2V_{SW}$, where V_{SW}=450 km s^{-1} is the solar wind speed at 1 AU. This spherical distribution function crosses the termination shock unchanged. Beyond the shock, the pickup protons are convected by the plasma flow field calculated for the two-shock gasdynamical model described above. In other words, no pickup proton heating and compression at the shock crossing occurs, and the pickup protons are not cooled as they are convected to the heliospheric tail. It is assumed here and in sections 8 and 9 that pickup protons constitute 15% of the solar wind at the termination shock.

Second, we assume that the same uniform spherical velocity distribution is thermalized into a Maxwellian distribution in the shock transition; no energy exchange occurs with the bulk of the solar wind plasma. The pickup protons can now be described by a shifted Maxwellian distribution function. In other words, we assume no heating and compression at the shock crossing, but the pickup proton energy is redistributed among the protons to form a Maxwellian distribution. This Maxwellian pickup proton population is convected to the heliospheric tail. We assume that the temperature of the pickup protons changes in proportion to the change of the bulk plasma temperature.

8. Imaging the Heliosphere in ENA Fluxes

The energy-angle dependences of ENA fluxes are shown in Plate 1. The axes are the ENA energy and the observation angle θ (see Figure 1) measured from the upwind direction. This format is convenient for an axisymmetric heliosphere and allows display of the whole sky for all ENA energies. The top panel of Plate 1 shows the energy-angle dependence of heliospheric ENAs for a strong gasdynamical shock.

The ENA flux peaks in the upwind direction. While ENAs with <0.2 keV account for most of the flux, the wings of the velocity distribution produce numerous energetic neutrals with the energies up to several keV (not seen with the color coding used). The typical energy distributions for four different directions are shown in Figure 7. Measurement of the ENA fluxes in a few bands in the 0.2-6 keV energy range would reliably establish the curve slopes. This range is also most important for probing the pickup protons in the heliosheath. In addition, ENAs in this energy range are readily detectable by the existing techniques. Therefore we concentrate on heliosphere ENA imaging in the 0.2-6 keV energy range.

A weak termination shock would show very different signatures in ENA fluxes. The bulk of the original solar wind plasma would only be slightly heated by the transition across the shock. Such heating is insufficient to produce the desired numbers of ENAs with the Sun-pointed velocities. However, the pickup protons would provide an excellent means to probe the interface region structure. Solar wind turbulence may increase the "diameter" of the pickup proton distribution sphere in the velocity space and extend the wings of the distribution. Recent estimates [*Fahr and Lay*, 2000] show that the energy spectrum of the pickup protons would depend on the solar wind turbulence level and may result in a relatively flat energy distribution up to the 5-keV energies. This will also be measurable.

The energy-angle ENA dependences for the two pickup proton evolution scenarios, as described in section 7, are shown in Plate 1 (middle and bottom panels). The middle panel shows the case of the pickup protons thermalized in the shock crossing. The pickup protons are convected into the tail with the temperature scaled (cooled) with the local temperature of the bulk plasma. The bottom panel shows the original spherical pickup proton distribution being convected by the two-shock model flow field without thermalization and without cooling. Possible compression of pickup protons in the shock crossing would result in slightly higher ENA fluxes.

The thermalized pickup proton population produces ENA distributions, not unlike those for the strongly shocked solar wind plasma but extending to much higher energies because of the significantly higher effective temperature of the protons. The distribution of the ENAs produced by nonthermalized pickup protons (Plate 1, bottom) shows an abrupt cutoff at high energies and strikingly different angular dependence. The cutoff energy in a given direction is determined by the maximum possible velocity of pickup protons and by the plasma radial velocity along the line of sight. Characteristically, the ENA flux peaks in the downwind hemisphere in the $120° < \theta < 150°$ range, which is an effect of the minimal radial plasma velocity and extended ENA-producing region in these directions. By measuring the energy cutoff and absolute ENA fluxes, one could determine the solar wind turbulence and its latitudinal dependence. The effects of the solar wind turbulence would be interwoven with the possible shock compression.

Representative all-sky ENA images in a selected energy band, 0.24 keV < *E* < 0.55 keV, are shown in Plate 2 in a conventional Mercator projection in the ecliptic coordinates with color coding of ENA fluxes. This and other energy bands are those of a realistic ENA single-pixel imager based on available technology and optimized for heliosphere imaging [*Funsten et al.*, 1998b].

For the gasdynamical strong shock case the ENA flux (cm^{-2} s^{-1} sr^{-1}) peaks in the upwind direction (ecliptic longitude 252° and latitude +7°) for the interstellar gas flow relative to the Sun

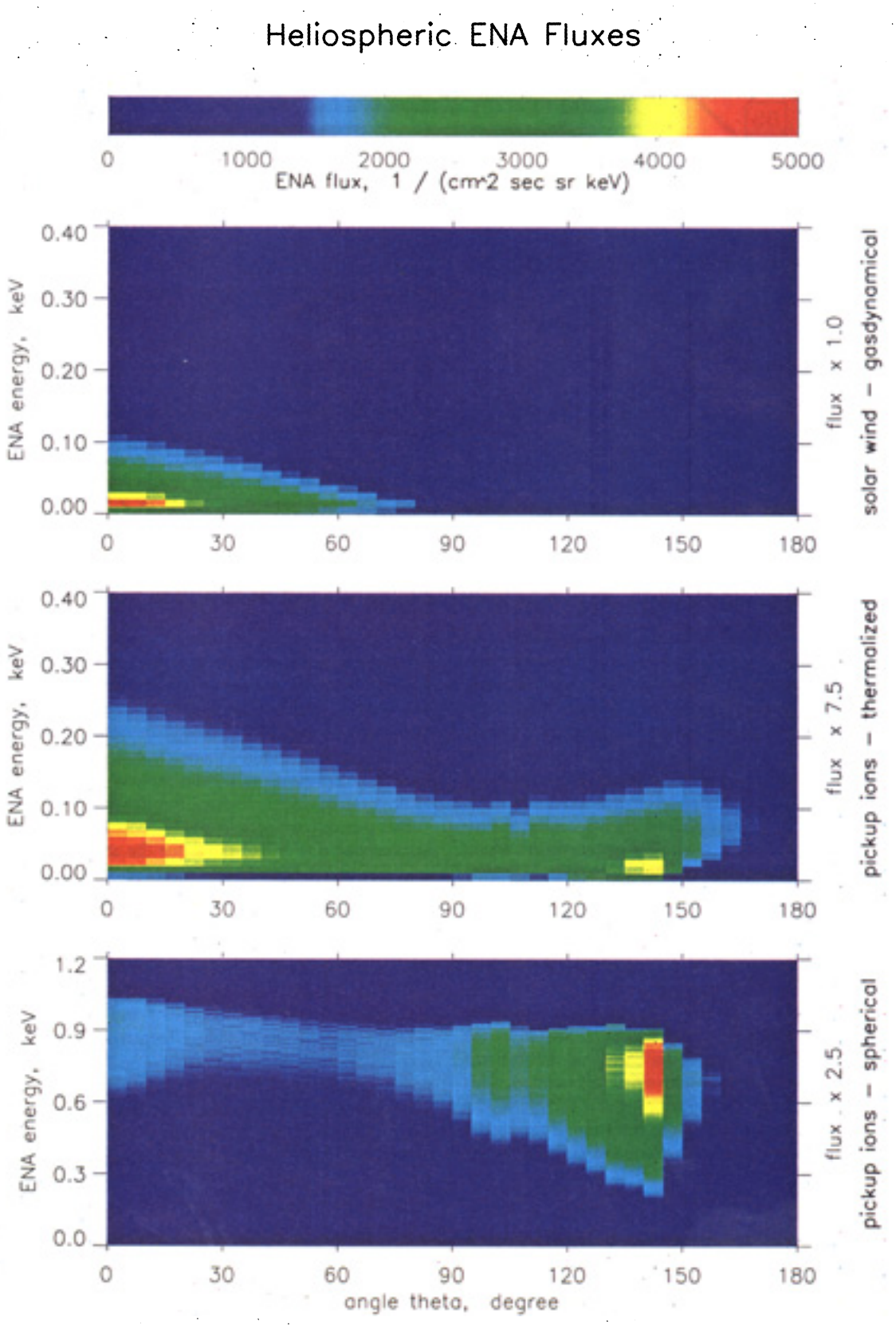

Plate 1. Energy-angle all-sky ENA images for (top) a strong gas-dynamical shock, (middle) a spherical isotropic pickup proton population with thermalization in the shock transition and cooling during convection to the heliospheric tail and (bottom) a spherical isotropic pickup proton population without thermalization and without cooling, Note that the fluxes are multiplied by 1.0, 7.5, and 2.5 for the top, middle, and bottom panels, respectively, to fit into the same color scale.

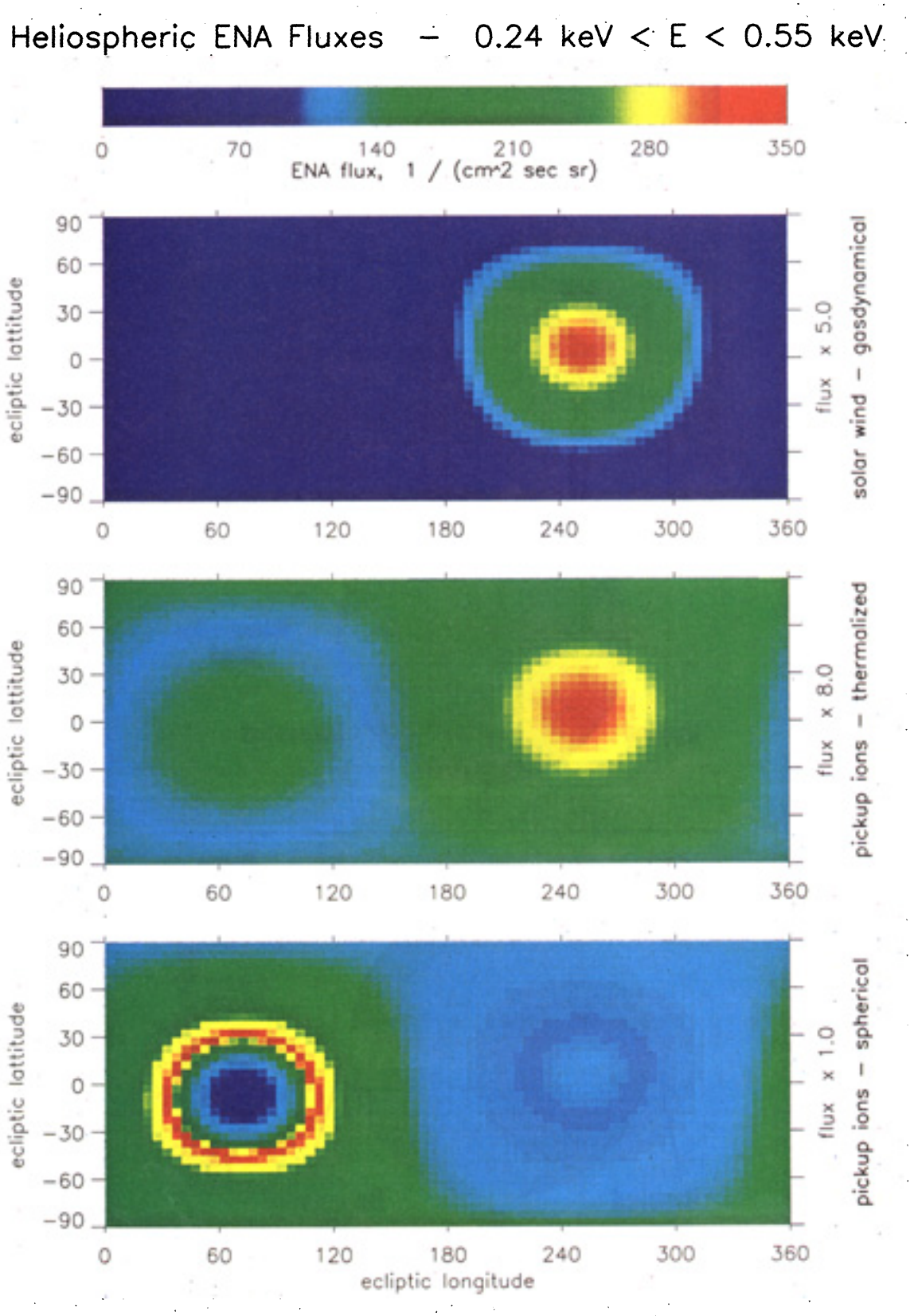

Plate 2. All-sky ENA images in the 0.24 keV < E < 0.55 keV energy band for (top) a strong gas-dynamical shock, (middle) a spherical isotropic pickup proton population with thermalization in the shock transition and cooling while being convected to the heliospheric tail, and (bottom) a spherical isotropic pickup proton population without thermalization and without cooling. Note that the fluxes are multiplied by 5.0, 8.0, and 1.0 for the top, middle, and bottom panels, respectively, to fit into the same color scale.

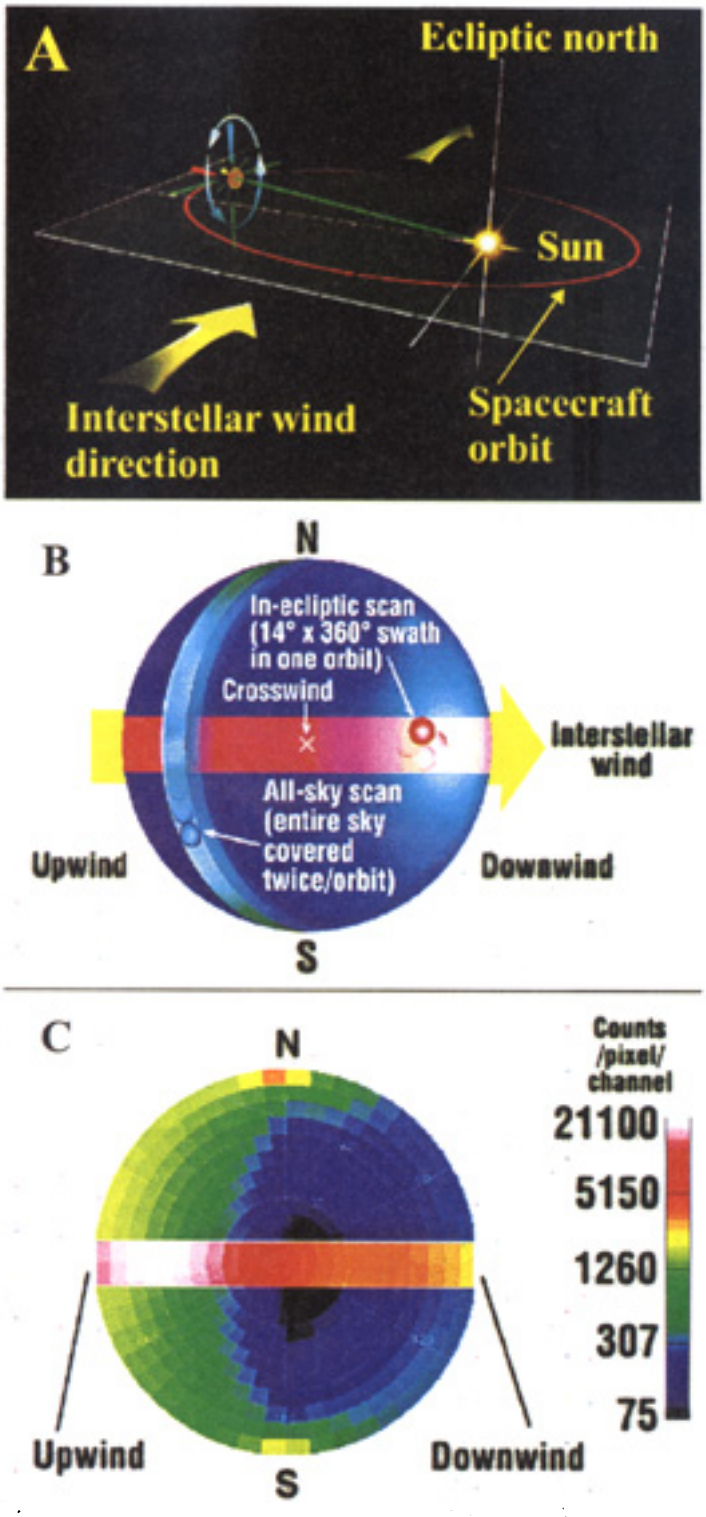

Plate 3. (a) A generic solar-cell-powered spacecraft in a heliocentric elliptical orbit in the ecliptic plane with a 3-year period. The orbit perihelion and aphelion are 1.0 and 3.1 AU, respectively, and the line of apsides is perpendicular to the direction of the interstellar wind flow. The spacecraft spin axis is pointed at the Sun. One ENA sensor is pointed normally to the spin axis, and the other is pointed parallel to the spin axis in the antisolar direction. (b) Covering of the celestial sphere by ENA sensors in a "fish-eye" projection centered on the direction cross-wind to the interstellar wind gas flow. (c) Total simulated ENA counts in each 7°×7° pixel over the 0.24 keV<E<0.55 keV energy channel during a nominal 3-year mission in the same hemisphere as that of Plate 3b.

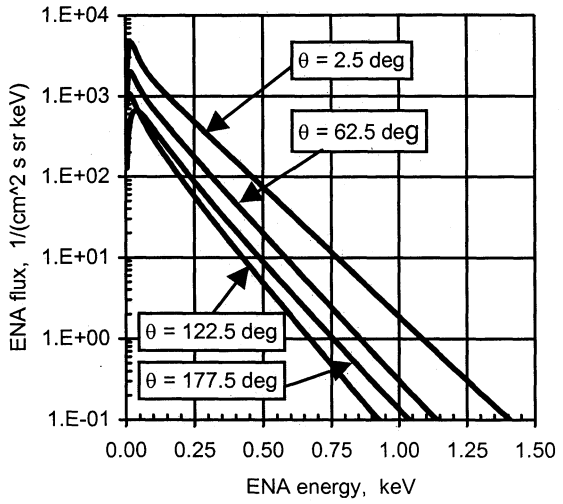

Figure 7. Energy dependence of ENA fluxes for four different directions for the strong-shock gasdynamical model. Angle θ is measured from the upwind direction.

(Plate 2, top). The gasdynamical heating is strongest at the nose of the heliosphere. The shocked flow stagnates in this region of the heliospheric sheath, before beginning to stream around the termination shock toward the tail. The radial component of the plasma velocity is thus reduced to an outward minimum. Under such conditions, the ENAs are generated by the protons in the core of the heated phase space distribution and can be observed at 1 AU at essentially the same energy as that their parent protons had in the plasma frame.

An ENA image of the thermalized pickup protons is expectedly similar to that of the strong-shock case but extends to much higher energies (Plate 2, middle). The secondary peak between θ = 120° and 180° is an effect of the plasma flow around the heliosphere with the extended ENA-producing region downwind. The ENA fluxes exhibit an entirely different image (Plate 2, bottom) in the case of the spherical velocity distribution of pickup protons without thermalization and without cooling. The fluxes peak in the downwind hemisphere in the shape of a broad annulus 70°-80° in diameter.

Figure 8 shows the ENA flux angular dependences in two energy bands ($0.24<E<0.55$ keV and $0.58<E<1.19$ keV) for a gasdynamical strong shock (curves A) and weak shock thermalized (curves B) and non-thermal (curves C) pickup protons. The striking differences in ENA fluxes and their angular behavior in various energy channels demonstrate how heliospheric ENA images reveal the nature of the processes in the heliospheric interface.

The strong-shock case angular dependence (curves A, Figure 8) illustrates an important ENA flux enhancement in the downwind region. This enhancement is a signature of the ENA-producing region stretching to large distances in the heliospheric tail. In the absence of ENA loss beyond the termination shock, the ENA flux (cm^{-2} sr^{-1} s^{-1}) would be proportional to the extension of the ENA-producing region. Figure 8 actually indicates a conservative estimate of the ENA flux enhancement, because the computational region was limited to 700 AU in this direction. The tail flux enhancement would stand out in an ENA celestial sphere map. (This enhancement is not seen in Plate 2, because of the limitations of the color coding used.) ENA imaging of the downwind hemisphere is a unique and highly promising way to explore the properties and extension of the heliospheric tail.

The observed solar wind asymmetry [*McComas et al.*, 2000a] would be prominently displayed as higher energies of the ENAs from the polar directions, corresponding to the higher solar wind velocities. The higher energies are expected for a gasdynamical shock scenario and for the ENAs produced by the solar wind pickup ions. The asymmetry of the interstellar magnetic field would lead to the north-south asymmetry of the heliospheric ENA images.

9. Heliosphere Imaging Mission and Instrumentation

The expected ENA fluxes are exceptionally weak. It may take more than a year to obtain an image of the heliosphere. An optimal approach seems to be to use a single-pixel ENA instrument with a large geometric factor to construct a composite image by scanning the sky by combining the spacecraft spinning and evolution of the pointing of the spacecraft spin axis. Optimization of such a complex approach is not trivial and requires careful planning and implementation. The feasibility study of an experiment to image the heliosphere in ENA fluxes [*Gruntman et al.*, 1999] was performed as a part of the development of the Interstellar Pathfinder mission [*Gloeckler et al.*, 1999]. A realistic single-pixel heliospheric ENA sensor has a field of view ~7°x7° and an effective geometric factor 0.001 cm^2 sr at 0.3 keV, 0.005 cm^2 sr at 0.9 keV, and 0.020 cm^2 sr at 6.0 keV [*Funsten et al.*, 1998b]. The energy range of interest, 0.2-6.0 keV, is covered by six contiguous energy bands, with the energy channel limits 0.24, 0.55, 1.2, 2.3, 3.8, and 5.9 keV, as shown in Figure 9.

The spacecraft should be well outside the magnetosphere, which is a copious source of ENAs at all energies of interest here. A spinning spacecraft is most desirable with the ENA instrument boresight pointed normally to the spin axis, to sweep a swath in the sky with each spin. If the spin axis precesses about an axis perpendicular to the spin axis over a period T, then the entire celestial sphere will be scanned in a half of that time, $T/2$.

A convenient way to achieve the desired experiment geometry is to point the spacecraft spin axis at the Sun. A generic solar-cell-powered spacecraft in a heliocentric elliptical orbit in the ecliptic plane with a 3-year period is sketched in Plate 3a [*Gloeckler et al.*, 1999; *Gruntman et al.*, 1999]. The orbit perihelion and aphelion are 1.0 and 3.1 AU, respectively, and the line of apsides is perpendicular to the direction of the interstellar wind flow. A 1-AU circular orbit around the Sun is also possible. The spacecraft spins about the axis pointed at the Sun, and the whole sky would be covered in 1 year and a half by an ENA sensor pointed normally to the spin axis. This observation scheme is illustrated in Plate 3b, which shows the sky hemisphere centered on the cross-wind direction, i.e., from the Sun toward the orbit aphelion (Plate 3a).

A second, identical ENA sensor is pointed close to the spin axis in the antisolar direction. One gains a bit more angular coverage about the ecliptic by cocking this "parallel" imager 3.5° off the antispin axis, so that it actually sweeps out a 14° angular band in the ecliptic plane. The sensor would allow detailed study of the processes near the ecliptic with the superb statistical accuracy. The normally pointed instrument covers various directions with an uneven duty cycle, with maximum

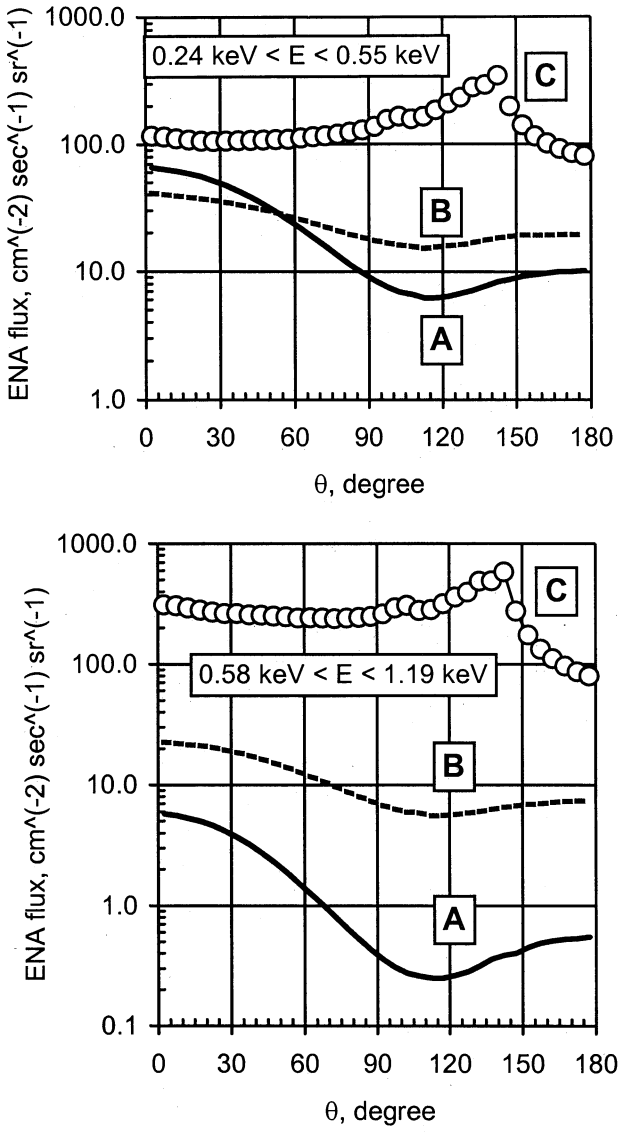

Figure 8. Angular dependence of ENA fluxes in the (top) 0.24 keV < E < 0.55 keV energy range and (bottom) 0.58 keV < E < 1.19 keV energy range. Curves A, strong gasdynamical shock; curves B, pickup protons Maxwellized (thermalized) in the shock transition and cooled while convected; and curves C, pickup protons without Maxwellization (thermalization) and without cooling.

duty cycle achieved for the polar heliospheric regions and minimal duty cycle achieved for the regions close to the ecliptic plane. The directional dependence of the coverage duty cycle is compensated for during the data reduction. Since both instruments would cover some identical directions in the sky during the mission, they can be intercalibrated.

The transverse (spinning) imager will cover the entire celestial sphere in half of the orbit period, $T/2$, but with a low duty cycle. On the other hand, the parallel imager will only sweep the ecliptic directions in the period T, but with ~50 times the duty cycle of the spinning imager. Much higher numbers of counts accumulated in ecliptic pixels are important for identifying possible contributions from nontermination shock ENA sources inside the heliosphere. This ENA foreground includes contributions from the energetic proton populations associated with shocks in the solar wind [*Roelof*, 1992].

For the 1×3.1 AU orbit the greatly reduced angular velocity of the spacecraft near aphelion produces the high exposure times (70 days per 7°×7° pixel) for the in-ecliptic imager in the cross-wind direction. The same orbital dynamic enhances the exposure times for the spinning all-sky imager in the upwind and downwind directions, relative to a 1-AU circular orbit. Thus the 1×3.1 AU orbit actually increases the sensitivity of the all-sky imager to the expected important upwind/downwind asymmetries in ENA fluxes. Similarly, the very high exposure time for the in-ecliptic head in the cross-wind direction opens the possibility of detecting temporal variations on the ecliptic flanks of the termination shock.

Plate 3c demonstrates total simulated ENA counts in the 0.24 keV<E<0.55 keV energy channel during a nominal 3-year mission. The counts in the 7°×7° pixels summed over the 3-year mission range from 75 to 21,100, yielding Poisson statistical uncertainties ranging from 11% down to 0.7%, respectively. The count enhancement from the upwind direction is expected because of the high ENA fluxes, while the brightening at the poles is an artifact of the exposure time pattern.

The expected count rates in different energy channels of the realistic instrument [*Funsten et al.*, 1998b] are shown in Figure 9. The steep spectrum from the gasdynamical termination shock would clearly stand out in the two lowest channels, while the upwind/downwind direction difference is easily detectable as a factor of 5:1 to 10:1 ratio in the counts within either of the lowest energy channels. Pickup-proton-produced ENAs would dominate the three highest energy channels, the spectral extension revealing the degree of the solar wind turbulence and compression in the termination shock.

The discussion of the instrumentation issues is beyond the scope of this article and this journal. We note that the instrumentation for ENA detection in the 0.2–6 keV energy range is well developed [*McComas et al.*, 1994; *Funsten et al.*, 1995; *Gruntman*, 1997]. The background counts are efficiently suppressed to the negligible levels by the coincidence technique [*Mitchell et al.*, 1993, 2000; *McComas et al.*, 1994; *Funsten et al.*, 1995; *Gruntman*, 1997; *Pollock et al.*, 2000], and the flux determination accuracy is dominated by the counting statistics.

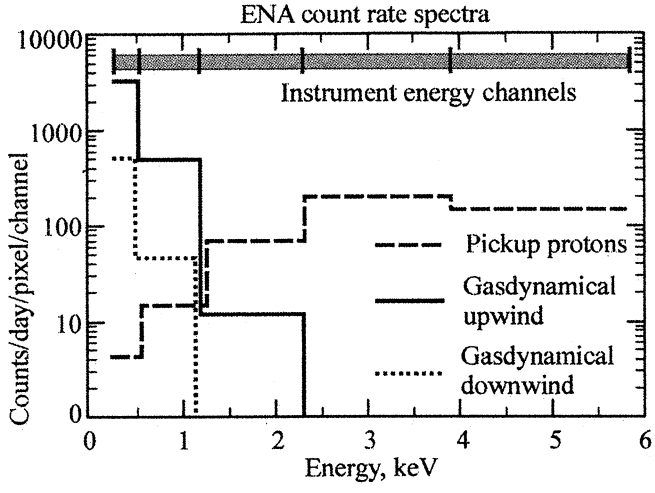

Figure 9. Calculated instrument ENA count rates for a strong (gasdynamical) shock in the upwind and downwind directions and for pickup protons (model of *Fahr and Lay* [2000]). The instrument energy channels are shown at the top of Figure 9.

The measurement technique is based on ionizing (stripping) ENAs by transmission through ultra-thin foils followed by the energy analysis of the ionized ENAs. The lower energy limit for the technique is determined by the stripping efficiency of the foils. The technique efficiently works down to the energies as low as 200-250 eV [*Overbury et al.*, 1979; *Funsten et al.*, 1994, 1998a, 1998b].

To conclude, ENA imaging is a powerful technique to remotely probe properties of distant hot plasmas. The technique ideally suits the study of the asymmetric, three-dimensional heliospheric interface. ENA imaging in the 0.2-6 keV energy range will establish the nature of the termination shock and properties of hot proton populations in the heliosheath. The evolution of pickup proton population at and beyond the shock can be remotely explored. Heliosphere ENA imaging would distinguish among the competing Sun-LISM interaction models and explore the physics of the critical processes in the interface region. Weak ENA fluxes make imaging implementation nontrivial, but it can be done, as we show, by single-pixel ENA sensors on a spinning spacecraft during a typical mission near 1 AU. The instrumentation technology is ready.

Acknowledgements. The authors thank Vladimir Baranov and his group for calculating the heliospheric plasma-gas structure for this work. The efforts of E. C. R. and D. G. M. were supported in part by grant NAG5-3879 from NASA to the Johns Hopkins University. Work at Los Alamos National Laboratory (H.O.F. and D.J.M.) was performed under auspices of the U.S. Department of Energy. M.G. was supported in part by NASA grant NAG5-6966.

Janet G. Luhmann thanks Earl Scime and another referee for their assistance in evaluating this paper.

References

Axford, W. I., The interaction of the solar wind with the interstellar medium, in *Solar Wind, NASA Spec. Publ., SP-308*, 609-660, 1972.

Axford, W. I., A. J. Dessler, and B. Gottlieb, Termination of solar wind and solar magnetic field, *Astrophys. J., 137*, 1268-1278, 1963.

Baranov, V. B., Gasdynamics of the solar wind interaction with the interstellar medium, *Space Sci. Rev., 52*, 89-120, 1990.

Baranov, V. B., and Y. G. Malama, The model of the solar wind interaction with the local interstellar medium: Numerical solution of self-consistent problem, *J. Geophys. Res., 98*, 15,157-15,163, 1993.

Baranov, V. B., and Y. G. Malama, Effect of local interstellar medium hydrogen fractional ionization on the distant solar wind and interface region, *J. Geophys. Res., 100*, 14,755-14,761, 1995.

Baranov, V.B., V.V. Izmodenov, and Y.G. Malama, On the distribution function of H-atoms in the problem of the solar wind interaction with the local interstellar medium, *J. Geophys. Res., 103*, 9575-9585, 1998.

Bertaux, J.-L., Helium and hydrogen of the local interstellar medium observed in the vicinity of the Sun, in *IAU Colloquium No.81, NASA Conf. Publ., CP 2345*, 3-23, 1984.

Bertaux, J.L., E. Quemerais, and R. Lallement, Observation of a sky Lyman α groove related to enhanced solar wind mass flux in the neutral sheet, *Geophys. Res. Lett., 23*, 3675-3678, 1996.

Bertaux, J.-L., E. Kyrölä, E. Quemerais, R. Lallement, W. Schmidt, T. Summanen, J. Costa, and T. Mäkinen, SWAN observations of the solar wind latitude distribution and its evolution since launch, *Space Sci. Rev., 87*, 129-132, 1999.

Bogdan, T.J., M.A. Lee, and P. Schneider, Coupled quasi-linear wave damping and stochastic acceleration of pickup ions in the solar wind, *J. Geophys. Res., 96*, 161-178, 1991.

Brandt, P. C., S. Barabash, O. Norberg, R. Lundin, E.C. Roelof, and C.J. Chase, Energetic neutral atom imaging at low altitudes from the Swedish microsatellite Astrid: Images and spectral analysis, *J. Geophys. Res.,104*, 2367-2380, 1999.

Breitschwerdt, D., The local bubble, *Space Sci. Rev., 78*, 173-182, 1996.

Chalov, S.V., and H.J. Fahr, A two-fluid model of the solar wind termination shock modified by shock-generated cosmic rays including energy losses, *Astron. Astrophys., 228*, 973-980, 1994.

Chalov, S.V., and H.J. Fahr, Reflection of preaccelerated pickup ions at the solar wind termination shock: The seed for anomalous cosmic rays, *Sol. Phys., 168*, 389-411, 1996.

Chalov, S.V., and H.J. Fahr, Pick-up ion acceleration at the termination shock and post-shock pick-up ion energy distribution, *Astron. Astrophys., 360*, 381-390, 2000.

Chalov, S.V., H.J. Fahr, and V. Izmodenov, Spectra of energized pick-up ions upstream of the 2-dimensional heliospheric termination shock, 1, The role of Alfvenic turbulences, *Astron. Astrophys., 304*, 609-616, 1995.

Chalov, S.V., H.J. Fahr, and V. Izmodenov, Spectra of energized pick-up ions upstream of the 2-dimensional heliospheric termination shock, 2, Acceleration by Alfvenic and by large-scale solar wind turbulences, *Astron. Astrophys., 320*, 659-671, 1997.

Cox, D.P., and R.J. Reynolds, The local interstellar medium, *Annu. Rev. Astron. Astrophys., 25*, 303-344, 1987.

Czechowski, A., S. Grzedzielski, and I. Mostafa, Apex-antiapex asymmetry in the anomalous cosmic ray distribution in the heliosheath, *Astron. Astrophys., 297*, 892-898, 1995.

Davis, L., Jr., Interplanetary magnetic fields and cosmic rays, *Phys. Rev., 100*, 1440-1444, 1955.

Dessler, A. J., Solar wind and interplanetary magnetic field, *Rev. Geophys., 5*, 1-41, 1967.

Fahr, H. J., On the influence of neutral interstellar matter on the upper atmosphere, *Astrophys. Space Sci., 2*, 474-495, 1968a.

Fahr, H. J., Neutral corpuscular energy flux by charge-transfer collisions in the vicinity of the Sun, *Astrophys. Space Sci., 2*, 496-503, 1968b.

Fahr, H.J., Non-thermal solar wind heating by suprathermal ions, *Sol. Phys., 30*, 193-206, 1973.

Fahr, H. J., The extraterrestrial UV-background and the nearby interstellar medium, *Space Sci. Rev., 15*, 483-540, 1974.

Fahr, H.J., The interstellar gas flow through the heliospheric interface region, *Space Sci. Rev., 78*, 199-212, 1996.

Fahr, H.J., and J. Ziemkiewicz, The behavior of distant heliospheric pick-up ions and associated solar wind heating, *Astron. Astrophys., 202*, 295-305, 1988.

Fahr, H.J., and H. Fichtner, Physical reasons and consequences of a three-dimensionally structured heliosphere, *Space Sci. Rev., 58*, 193-258, 1991.

Fahr, H.J., and D. Rucinski, Neutral interstellar gas atoms reducing the solar wind Mach number and fractionally neutralizing the solar wind, *Astron. Astrophys., 350*, 1071-1078, 1999.

Fahr, H.J., and G. Lay, Remote diagnostic of the heliospheric termination shock using neutralized post-shock pick-up ions as messengers, *Astron. Astrophys., 356*, 327-334, 2000.

Fahr, H.J., R. Osterbart, and D. Rucinski, Modulation of the interstellar oxygen-to-hydrogen ratio by the heliospheric interface plasma, *Astron. Astrophys., 294*, 587-600, 1995.

Fahr, H.J., T. Kausch, and H. Scherer, A 5-fluid hydrodynamic approach to model the solar system-interstellar medium interaction, *Astron. Astrophys., 357*, 268-282, 2000.

Fisk, L.A., Implications of a weak termination shock, *Space Sci. Rev., 78*, 129-136, 1996.

Fisk, L.A., B. Kozlovsky, and R. Ramaty, An interpretation of the observed oxygen and nitrogen enhancements in low-energy cosmic rays, *Astrophys. J., 190*, L35-L37, 1974.

Frisch, P.C., Characteristics of nearby interstellar matter, *Space Sci. Rev., 72*, 499-592, 1995.

Funsten, H.O., D.J. McComas, and E.E. Scime, Comparative study of low energy neutral atom imaging techniques, *Opt. Eng., 33*, 349-356, 1994.

Funsten, H.O., D.J. McComas, and E.E. Scime, Low-energy neutral-atom imaging techniques for remote observations of the magnetosphere, *J. Spacecr. Rockets, 32*, 899-904, 1995.

Funsten, H.O., D.J. McComas, and M.A. Gruntman, Neutral atom imaging: UV rejection techniques, in *Measurement Techniques in Space Plasmas: Fields, Geophys. Monogr. Ser.*, Vol.103, edited by R. Pfaff, J. Borovsky, and D.T. Young, pp. 251-256, AGU, Washington, 1998a.

Funsten, H.O., D.J. McComas, D.G. Mitchell, E. C. Roelof, and M.A. Gruntman, Energetic neutral atoms imaging of the heliospheric termination shock, *Eos Trans. AGU, 79*(45), Fall Meet. Suppl., F705, 1998b.

Gloeckler, G., J. Geiss, H. Balsiger, L. A. Fisk, A. B. Galvin, F. M. Ipavich, K. W. Ogilvie, R. von Steiger, and B. Wilken, Detection of interstellar pickup hydrogen in the solar system, *Science, 261*, 70-73, 1993.

Gloeckler, G., J. Geiss, E.C. Roelof, L.A. Fisk, F.M. Ipavich, K.W. Ogilvie, L.J. Lanzerotti, R. von Steiger, and B. Wilken, Acceleration of interstellar pickup ions in the disturbed solar wind observed on Ulysses, *J. Geophys. Res.*, *99*, 17,637-17,643, 1994.

Gloeckler, G., E.C. Roelof, K.W. Ogilvie, and D.B. Berdichevsky, Proton phase space densities (0.5 eV < *Ep* < 5 MeV) at mid-latitudes from Ulysses SWICS/HI-SCALE measurements, *Space Sci. Rev.*, *72*, 321-326, 1995.

Gloeckler, G., L.A. Fisk, T.H. Zurbuchen, E. Moebius, H.O. Funsten, M. Witte, and E.C. Roelof, Interstellar Pathfinder: A mission to the inner edge of the interstellar medium, *Eos Trans. AGU*, *80*(17), Spring Meet. Suppl., S237, 1999.

Gruntman, M. A., Effect of neutral component of solar wind on the interaction of the solar system with the interstellar gas flow, *Sov. Astron. Lett.*, *8*(1), 24-26, 1982.

Gruntman, M. A., Anisotropy of the energetic neutral atom flux in the heliosphere, *Planet. Space Sci.*, *40*, 439-445, 1992.

Gruntman, M. A., Neutral solar wind properties: Advance warning of major geomagnetic storms, *J. Geophys. Res.*, *99*, 19,213-19,227, 1994.

Gruntman, M., Energetic neutral atom imaging of space plasmas, *Rev. Sci. Instrum.*, *68*, 3617-3656, 1997.

Gruntman, M., Imaging the three-dimensional solar wind, *J. Geophys. Res.*, *106*. 8205-8216, 2001a.

Gruntman, M., Mapping the heliopause in EUV, in *Proceedings of the COSPAR Colloquium on the Physics of the Outer Heliosphere*, Elsevier Sci., New York, in press, 2001b.

Gruntman, M., and H.J. Fahr, Access to the heliospheric boundary: EUV-echoes from the heliopause, *Geophys. Res. Lett.*, *25*, 1261-1264, 1998.

Gruntman, M., and H.J. Fahr, Heliopause imaging in EUV: Oxygen O^+ ion 83.4-nm resonance line emission, *J. Geophys. Res.*, *105*, 5189-5200, 2000.

Gruntman, M.A., V.B. Leonas, and S. Grzedzielski, Neutral solar wind experiment, in *Physics of the Outer Heliosphere*, edited by S. Grzedzielski and D.E. Page, pp..355-358, Pergamon, Tarrytown, N.Y., 1990.

Gruntman, M.A., E.C. Roelof, D.G. Mitchell, H.O. Funsten, D.J. McComas, and H.-J. Fahr, Energetic neutral atom imaging of the heliospheric termination shock and interface region on the "Interstellar Pathfinder" mission, *Eos Trans. AGU*, *80*(17), Spring Meet. Suppl., S237, 1999.

Henderson, M.G., G.D. Reeves, H.E. Spence, R.B. Sheldon, A.M. Jorgensen, J.B. Blake, and J.F. Fennel, First energetic neutral atom images from Polar, *Geophys. Res. Lett.*, *24*, 1167-1170, 1997.

Hilchenbach, M., et al., Detection of 55-80 keV hydrogen atoms of heliospheric origin by CELIAS/HSTOF on *SOHO*, *Astrophys. J.*, *503*, 916-922, 1998.

Holzer, T. E., Neutral hydrogen in interplanetary space, *Rev. Geophys..*, *15*, 467-490, 1977.

Holzer, T.E., and W.I. Axford, Solar wind ion composition, *J. Geophys. Res.*, *75*, 6354-6359, 1970.

Hsieh, K. C., and M. A. Gruntman, Viewing the outer heliosphere in energetic neutral atoms, *Adv. Space Res.*, *13*(6), 131-139, 1993.

Hsieh, K. C., K. L. Shih, J. R. Jokipii, and S. Grzedzielski, Probing the heliosphere with energetic neutral atoms, *Astrophys. J.*, *393*, 756-763, 1992.

Isenberg, P.A., Interaction of the solar wind with interstellar neutral hydrogen: Three-fluid model, *J. Geophys. Res.*, *91*, 9965-9972, 1986.

Isenberg, P.A., A hemispherical model of anisotropic interstellar pickup ions, *J. Geophys. Res.*, *102*, 4719-4724, 1997a.

Isenberg, P.A., A weaker solar wind termination shock, *Geophys. Res. Lett.*, *24*, 623-626, 1997b.

Izmodenov, V., Y.G. Malama, and R. Lallement, Interstellar neutral oxygen in a two-shock heliosphere, *Astron. Astrophys.*, *317*, 193-202, 1997.

Jaeger, S., and H.J. Fahr, The heliospheric plasma tail under influence of charge exchange processes with interstellar H-atoms, *Sol. Phys.*, *178*, 631-656, 1998.

Jokipii, J.R., and J. Giacalone, The acceleration of pickup ions, *Space Sci. Rev.*, *78*, 137-148, 1996.

Keppler, E., M. Franz, A. Korth, M.K. Reuss, J.B. Blake, R. Seidel, J.J. Quenby, and M. Witte, Observations of energetic particles with EPAC on Ulysses in polar latitude of the heliosphere, *Science*, *268*, 1013-1016, 1995.

Krimigis, S. M., et al., Magnetosphere Imaging Instrument (MIMI) on the Cassini Mission to Saturn/Titan, *Space Sci. Rev.*, in press, 2001.

Lallement, R., J.-L. Bertaux, E. Chassefiere, and B.R. Sandel, Lyman-alpha observations from Voyager (1-18 AU), in *Physics of the Outer Heliosphere*, edited by S. Grzedzielski and D.E. Page, pp.73-82, Pergamon, Tarrytown, N.Y., 1990.

Lallement, R., J.-L. Bertaux, and J.T. Clarke, Deceleration of interstellar hydrogen at the heliospheric interface, *Science*, *260*, 1095-1098, 1993.

Lee, M.A., The termination shock of the solar wind, *Space Sci. Rev.*, *78*, 109-116, 1996.

LeRoux, J.A. and H. Fichtner, The influence of pickup, anomalous, and galactic cosmic-ray protons on the heliospheric shock: A self-consistent approach, *Astrophys. J. Lett.*, *477*, L115-L118, 1997.

Linde, T.J., T.I. Gombosi, P.L. Roe, K.G. Powell, and D.L. DeZeeuw, Heliosphere in the magnetized local interstellar medium: Results of a 3-dimensional MHD simulation, *J. Geophys. Res.*, *103*, 1889-1904, 1998.

Linsky, J.L., S. Redfield, B.E. Wood, and N. Piskunov, The three-dimensional structure of the warm local interstellar medium, I, Methodology, *Astrophys. J.*, *528*, 756-766, 2000.

McComas, D.J., H.O. Funsten, J.T. Gosling, K.R. Moore, E.E. Scime, and M.F. Thomsen, Fundamentals of low-energy neutral atom imaging, *Opt. Eng.*, *33*, 335-341, 1994.

McComas, D.J., H.O. Funsten, J.T. Gosling, and W.R. Pryor, Ulysses measurements of variations in the solar wind-interstellar hydrogen charge exchange rate, *Geophys. Res. Lett.*, *26*, 2701-2704, 1999.

McComas, D.J., B.L. Barraclough, H.O. Funsten, J.T. Gosling, E. Santiago-Muñoz, R.M. Skoug, B.E. Goldstein, M. Neugebauer, P. Riley, and A. Balogh, Solar wind observations over Ulysses' first full polar orbit, *J. Geophys. Res.*, *105*, 10,419-10,433, 2000a.

McComas, D.J., J.T. Gosling, and R.M. Skoug, Ulysses observations of the irregularly structured mid-latitude solar wind during the approach to solar minimum, *Geophys. Res. Lett.*, *27*, 2437-2440, 2000b.

Meier, R. R., Some optical and kinetic properties of the nearby interstellar gas, *Astron. Astrophys.*, *55*, 211-219, 1977.

Mitchell, D. G., et al., INCA: The ion neutral camera for energetic neutral atom imaging of the Saturnian magnetosphere, *Opt. Eng.*, *32*, 3096-3101, 1993.

Mitchell, D.G., et al., High energy neutral atom (HENA) imager for the IMAGE mission, *Space Sci. Rev.*, *91*, 67-112, 2000.

Moebius, E., D. Hovestadt, B. Klecker, M. Scholer, G. Gloeckler, and F.M. Ipavich, Direct observation of He^+ pickup ions of interstellar origin in the solar wind, *Nature*, *318*, 426-429, 1985.

Moore, T.E., et al., Low energy neutral atom (LENA) imager for IMAGE, *Space Sci. Rev.*, *91*, 155-195, 2000.

Morton, D. C., and J. D. Purcell, Observations of the extreme ultraviolet radiation in the night sky using an atomic hydrogen filter, *Planet. Space Sci.*, *9*, 455-458, 1962.

Neugebauer, M., The three-dimensional solar wind at solar activity minimum, *Rev. Geophys.*, *37*, 107-126, 1999.

Orsini, S., et al., Proposal of an Italian experiment for the mission SAC-B. ISENA: Imaging particle spectrometer for energetic neutral atoms, in *Instrumentation for Magnetospheric Imagery*, edited by S. Chakrabarti, *Proc. SPIE Int. Soc. Opt. Eng.*, *1744*, 91-101, 1992

Osterbart, R., and H.J. Fahr, A Boltzmann-kinetic approach to describe the entrance of neutral interstellar hydrogen into the heliosphere, *Astron. Astrophys.*, *264*, 260-269, 1992.

Overbury, S. H., P. F. Dittner, S. Datz, and R. S. Thoe, Energy loss, angular distributions and charge fractions of low energy hydrogen transmitted through thin carbon foils, *Radiat. Eff.*, *41*, 219-227, 1979.

Parker, E.N., *Interplanetary Dynamical Processes*, Wiley-Interscience, New York, 1963.

Patterson, T. N. L., F. S. Johnson, and W. B. Hanson, The distribution of interplanetary hydrogen, *Planet. Space Sci.*, *11*, 767-778, 1963.

Pesses, M.E., J.R. Jokipii, and D. Eichler, Cosmic ray drift, shock wave acceleration, and the anomalous component of cosmic rays, *Astrophys. J. Lett.*, *246*, L85-L88, 1981.

Pollock, C.J., et al., Medium energy neutral atom (MENA) imager for the IMAGE mission, *Space Sci. Rev.*, *91*, 113-154, 2000.

Ratkiewicz, R., A. Barnes, G.A. Molvik, J.R. Spreiter, S.S. Stahara, M. Vinokur, and S. Venkateswaran, Effect of varying strength and orientation of local interstellar magnetic field on configuration of

exterior heliosphere: 3D MHD simulations, *Astron. Astrophys.*, *335*, 363-369, 1998.

Ripken, H.W., and H.J. Fahr, Modification of the local interstellar gas properties in the heliospheric interface, *Astron. Astrophys.*, *122*, 181-192, 1983.

Roelof, E. C., Energetic neutral atom image of a storm-time ring current, *Geophys. Res. Lett.*, *14*, 652-655, 1987.

Roelof, E. C., Imaging heliospheric shocks using energetic neutral atoms, in *Solar Wind Seven*, edited by E. Marsch and R. Schwenn, pp.385-394, Pergamon, Tarrytown, N.Y., 1992.

Roelof, E.C., D.G. Mitchell, and S.M. Krimigis, ENA images from the ion and neutral camera (INCA) during the Cassini Earth flyby, *Eos Trans. AGU*, *80*(46), Fall Meet. Suppl., F872, 1999.

Rucinski, D., A.C. Cummings, G. Gloeckler, A.J. Lazarus, E. Möbius, and M. Witte, Ionization processes in the heliosphere: Rates and methods of their determination, *Space Sci. Rev.*, *78*, 73-84, 1996.

Suess, S.T., The heliopause, *Rev. Geophys.*, *28*, 97-115, 1990.

Suess, S.T., Temporal variations in the termination shock distance, *J. Geophys. Res.*, *98*, 15,147-15,155, 1993.

Thomas, G. E., The interstellar wind and its influence on the interplanetary environment, *Annu. Rev. Earth Planet. Sci.*, *6*, 173-204, 1978.

Vasyliunas, V.M., and G.L. Siscoe, On the flux and the energy spectrum of interstellar ions in the solar system, *J. Geophys. Res.*, *81*, 1247-1252, 1976.

Wallis, M., Local interstellar medium, *Nature*, *254*, 202-203, 1975.

Williams, D. J., E. C. Roelof, and D. G. Mitchell, Global magnetosphere imaging, *Rev. Geophys.*, *30*, 183-208, 1992.

Witte, M., M. Banaszkiewicz, and H. Rosenbauer, Recent results on the parameters of the interstellar helium from the Ulysses/GAS experiment, *Space Sci. Rev.*, *78*, 289-296, 1996.

Wood, B.E., and J.L. Linsky, The local ISM and its interaction with the winds of nearby late-type stars, *Astrophys. J.*, *492*, 788-803, 1998.

Yoon, P.H., L.F. Ziebell, and C.S. Wu, Self-consistent pitch angle diffusion of newborn ions, *J. Geophys. Res.*, *96*, 5469-5478, 1991.

Zank, G.P, Interaction of the solar wind with the local interstellar medium: A theoretical perspective, *Space Sci. Rev.*, *89*, 1-275, 1999.

Zank, G.P., G.M. Web, and D.J. Donohue, Particle injection and the structure of energetic-particle-modified shocks, *Astrophys. J.*, *406*, 67-91, 1993.

Zank, G.P., H.L. Pauls, I.H. Cairns, and G.M. Webb, Interstellar pickup ions and quasi-perpendicular shocks: Implications for the termination shock and interplanetary shocks, *J. Geophys. Res.*, *101*, 457-477, 1996.

H.J. Fahr, Institut für Astrophysik und Extraterrestrische Forschung, Universität Bonn, Bonn D-53121, Germany.

H.O. Funsten, Los Alamos National Laboratory, Los Alamos, NM 87545.

M. Gruntman, Department of Aerospace and Mechanical Engineering, MC-1191, University of Southern California, Los Angeles, CA 90089-1191. (mikeg@spock.usc.edu)

D.J. McComas, Southwest Research Institute, San Antonio, TX 78228-0510.

D.G. Mitchell and E.C. Roelof, Applied Physics Laboratory, Johns Hopkins University, Laurel, MD 20707-6099.

(Received August 27, 2000; revised October 16, 2000;
accepted October 23, 2000.)